ASER INTERFEROMETER GRAVITATIONAL WAVE OBSERVATORY

LIGO

CALIFORNIA INSTITUTE OF TECHNOLOGY
MASSACHUSETTS INSTITUTE OF TECHNOLOGY

LIGO- **T1300731** -v1 13 September 2013

Low-Scatter Coating for Stainless Steel Baffles

Michael Smith

LIGO Hanford Observatory
P.O. Box 1970; Mail Stop S9-02
Richland, WA 99352
Phone (509) 37208106
Fax (509) 372-8137
E-mail: info@ligo.caltech.edu

LIGO Livingston Observatory
19100 LIGO Lane
Livingston, LA 70754
Phone (225) 686-3100
Fax (225) 686-7189
E-mail: info@ligo.caltech.edu

California Institute of Technology
LIGO – MS 100-36
Pasadena, CA 91125
Phone (626) 395-2129
Fax (626) 304-9834
E-mail: info@ligo.caltech.edu

Massachusetts Institute of Technology
LIGO – MS NW22-295
Cambridge, MA 02139
Phone (617) 253-4824
Fax (617) 253-7014
E-mail: info@ligo.mit.edu

CHANGE LOG

Date, version	Summary of Changes
8/27/13 V1	• New document

Table of Contents

Table of Figures

1 Introduction

An improved low-scattering and low-reflectivity coating for polished stainless steel was developed using a multilayer dielectric antireflection coating; the coating was applied by a commercial coating vendor using an ion assisted physical vapor deposition (PVD) process, in which an electron beam was used to evaporate the coating materials.

The BRDF and reflectance properties of the sample film were measured. The back-scatter BRDF at 57 deg incidence angle of the multilayer AR coating on SS is <1E-5 sr^-1 for p-polarization. The reflectivity of the multilayer AR coating on SS for 57 deg incidence angle is <1E-3 for both polarizations--i.e. > 99.9% of the incident power striking the louver portion of the ACB will be absorbed. This would be a very efficient baffle surface.

As an example of the use of this coating, the calculated scattered light noise from the aLIGO stainless steel Arm Cavity Baffle (ACB) with this multi-layer dielectric antireflection coating (mAR) is compared with a diamond-like coating (DLC), and with the aLIGO default oxidized stainless steel. An 80 times reduction in scattered light displacement noise could be obtained with the multilayer AR coating over the default oxidized SS ACB; whereas, a 19 times reduction in scattered light displacement noise could be achieved with the DLC coating.

One caveat of the use of the multi-layer dielectric antireflection coating is that it probably will be restricted to a planar surface; whereas, the DLC coating can be applied to an arbitrarily shaped surface.

1.1 ACB Scattering Surfaces

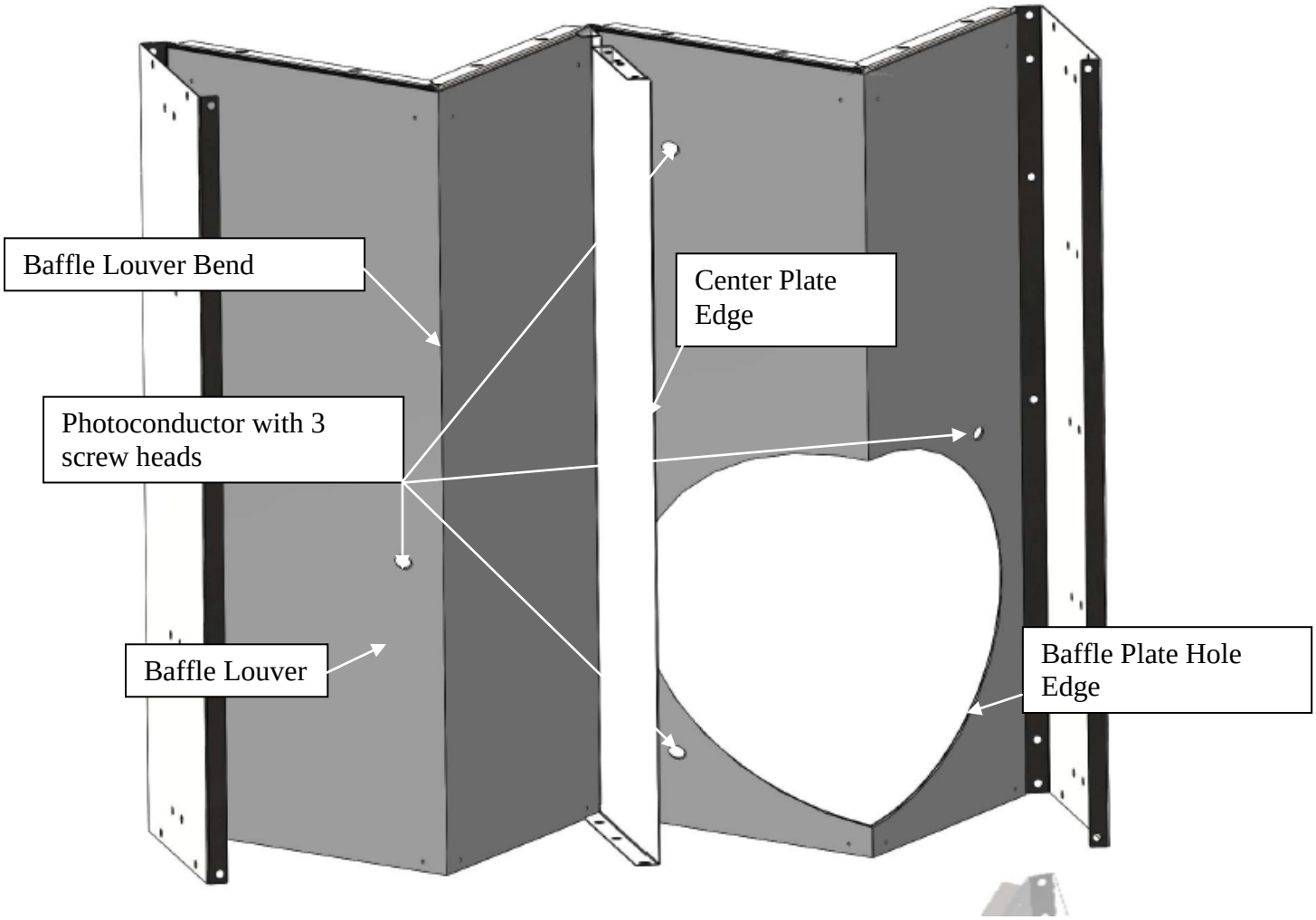

Figure 1: Arm Cavity Baffle Showing Principal Scattering Surfaces

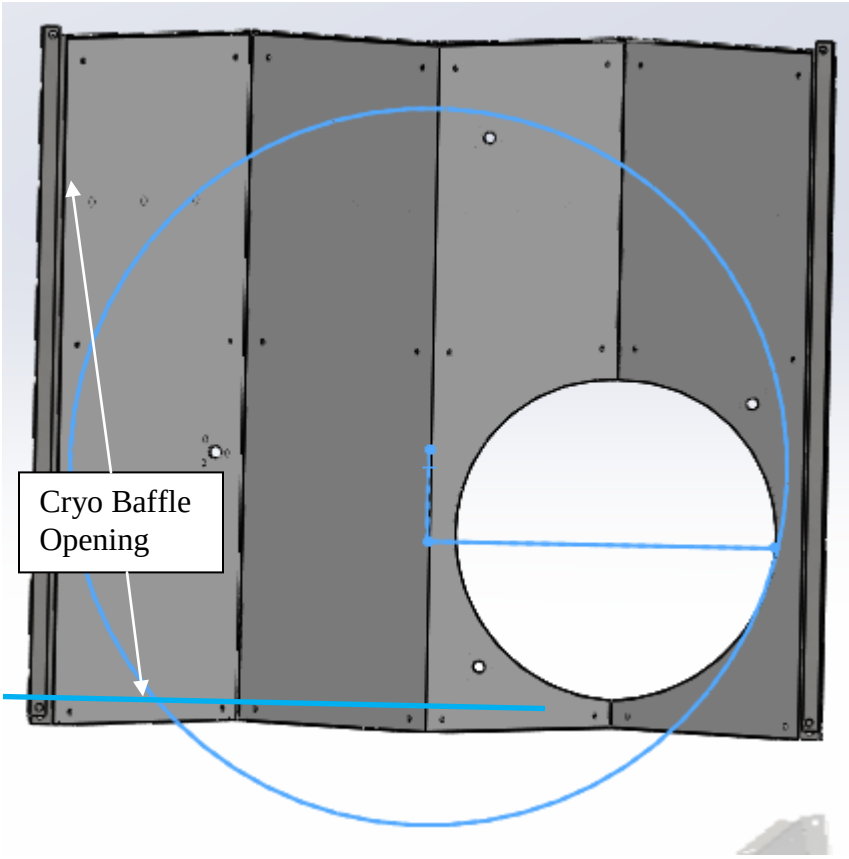

Figure 2: Frontal Area of ACB Hit by Narrow Angle Scatter from Far Test Mass Mirror

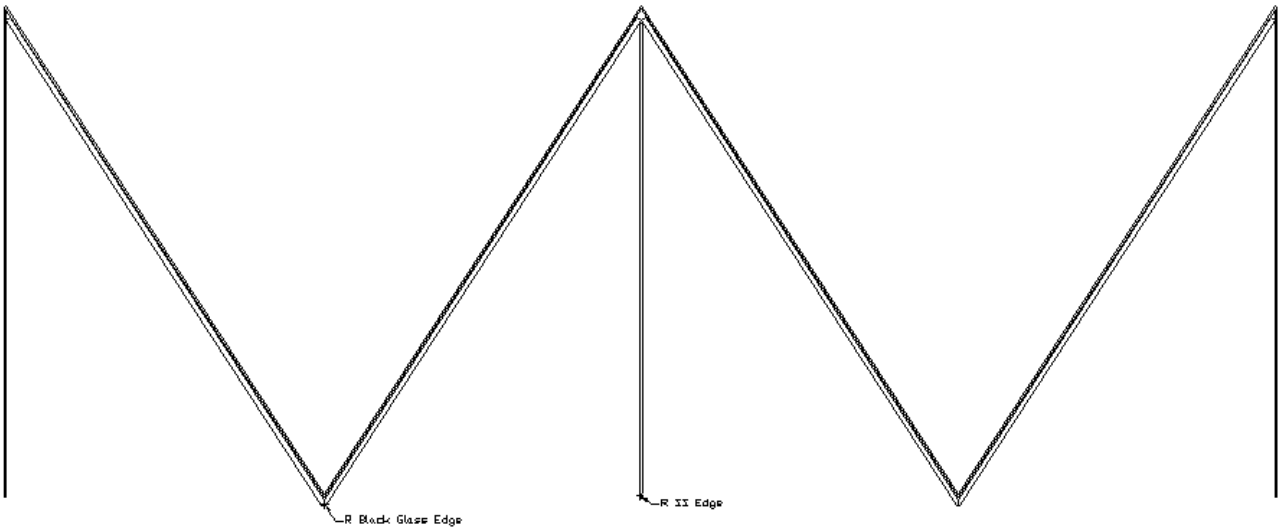

Figure 3: Cross-section of ACB

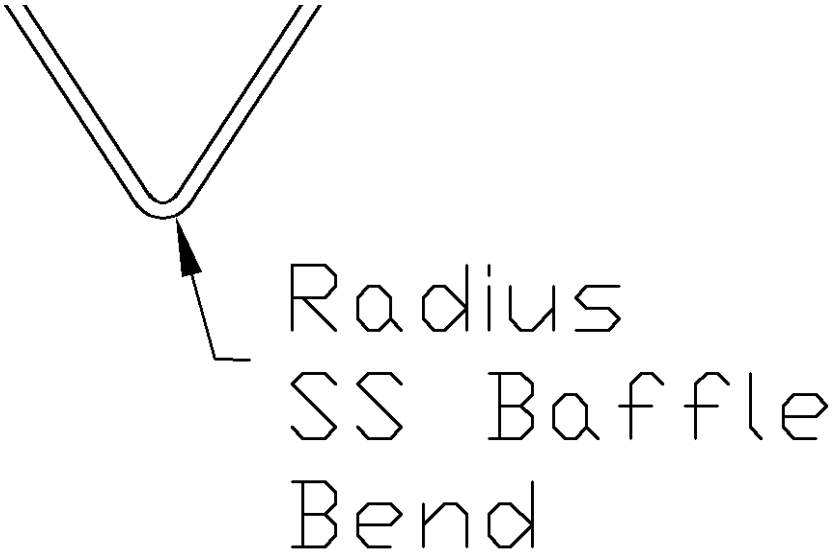

Figure 4: Bend Radius of ACB Used in the Scattered Light Calculation

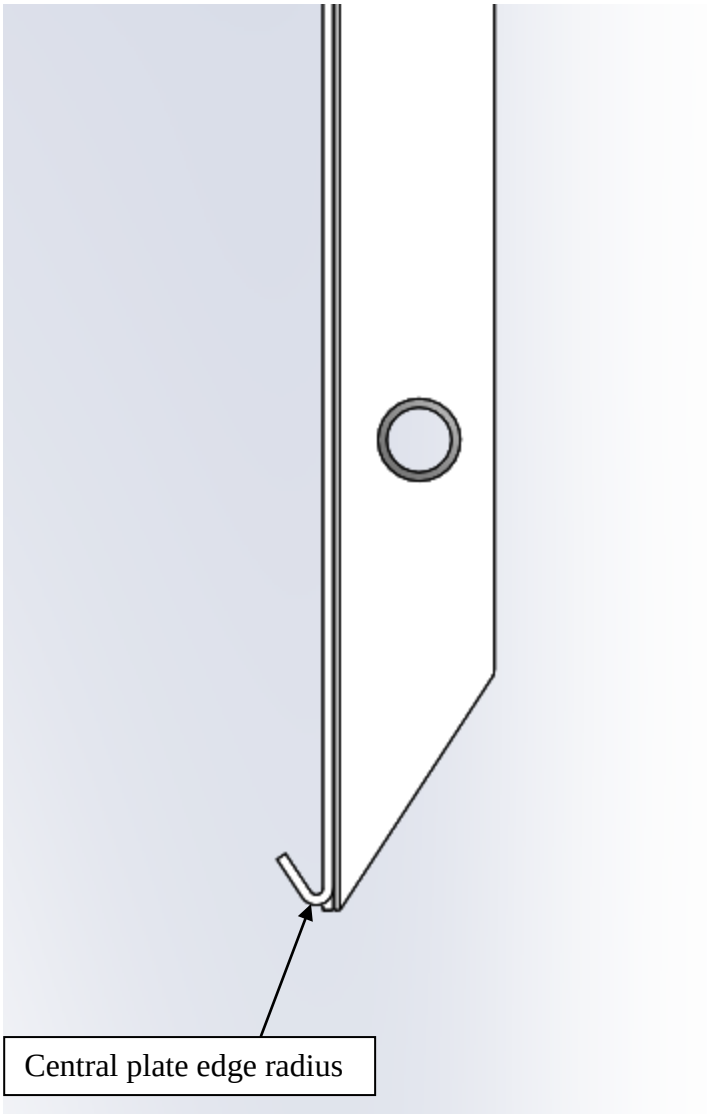

Figure 5: Edge Radius of Central Plate Used in the Scattered Light Calculation

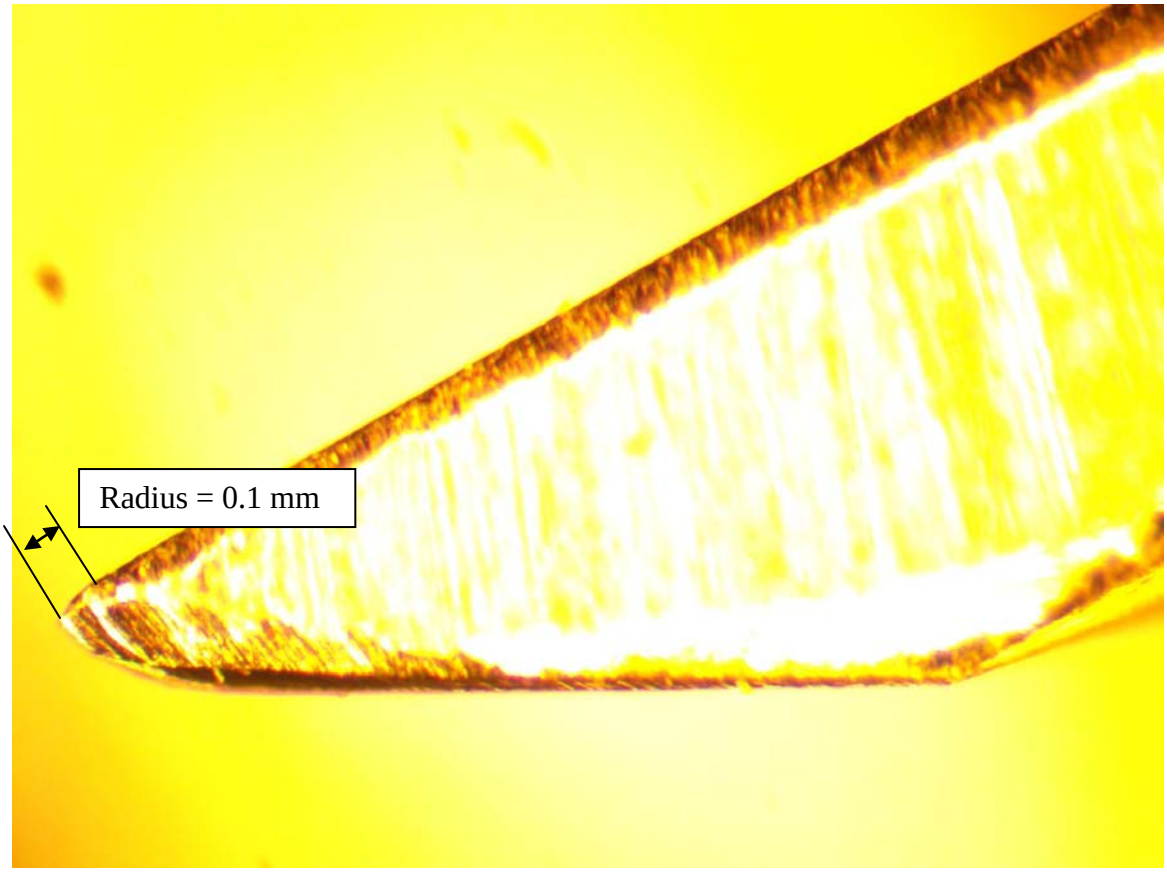

Figure 6: Actual Cross Section of ACB SS Hole Beveled Edge

2 Scattering Analysis

The scattered light from the surface of the far test mass mirror will pass down the interferometer arm, through the Manifold/Cryopump Baffle, and hit the Arm Cavity Baffle (ACB) in front of the near test mass.

2.1 Scattering Parameters

Arm Power, W

$$P_0 := 834174$$

radius of SS baffle edge, m

$$r_{edgess} := 0.00005$$

radius of SS baffle bend, m

$$r_{bendss} := 0.0024$$

length of baffle plate edge, m

$$H_p := 0.655$$

length of baffle bend, m

$$H_b := 2 \cdot 0.239 = 0.478$$

Frontal area of SS center plate cut edge, m^2

$$A_{ssbp}(r_{edgess}) := 2 \cdot r_{edgess} \cdot H_p$$

$$A_{ssbp}(r_{edgess}) = 6.55 \times 10^{-5}$$

Frontal area of SS baffle bend edge, m^2

$$A_{ssb}(r_{bendss}) := 2 \cdot r_{bendss} \cdot H_b$$

$$A_{ssb}(r_{bendss}) = 2.294 \times 10^{-3}$$

BRDF of SS cut edge, sr^-1

$$BRDF_{edgess} := 0.1$$

BRDF of photodetector, sr^-1

$$BRDF_{pd} := 1 \cdot 10^{-3}$$

BRDF of screw head sr^-1

$$BRDF_{sh} := 5 \cdot 10^{-2}$$

number of photodetector

$$N_{pd} := 16$$

number of screw heads

$$N_{sh} := 3 \cdot N_{pd}$$

radius of photodetector ring, m

$$r_{pdbc} := 0.196$$

Photoconductor radius, m

$$r_{pd} := \frac{0.0114}{2}$$

$$r_{pd} = 5.7 \times 10^{-3}$$

photoconductor area, m^2

$$A_{pd} := \pi \cdot r_{pd}^{2}$$

$$A_{pd} = 1.021 \times 10^{-4}$$

Screw head radius (#10), m

$$r_{sh} := .004$$

Screw head area, m^2

$$A_{sh} := \pi \cdot r_{sh}^{2}$$

$$A_{sh} = 5.027 \times 10^{-5}$$

laser wavelength, m

$$\lambda := 1.064 \cdot 10^{-6}$$

wave number, m^-1

$$k := 2 \cdot \frac{\pi}{\lambda}$$

$$k = 5.905 \times 10^{6}$$

ACB displacement @ 100 HZ, m/rt HZ

$$x_{ACB} := 1 \cdot 10^{-12}$$

IFO waist size, m

$$w_{ifo} := 0.012$$

solid angle of IFO mode, sr

$$\Delta\Omega_{ifo} := \frac{\lambda^{2}}{\pi \cdot w_{ifo}^{2}} = 2.502 \times 10^{-9}$$

Transfer function @ 100 Hz, ITM HR

$$TF_{itmhr} := 1.1 \cdot 10^{-9}$$

IFO arm length, m

$$L_{arm} := 4000$$

PSL laser power, W

$$P_{psl} := 125$$

Arm Power, W

$$P_0 := 834174$$

radius of Cryopump aperture, m

$$R_{cp} := 0.3845$$

half-angle from centerline to Rcp, rad

$$\theta_{cp} := \frac{R_{cp}}{L_{arm}}$$

half-angle from centerline to Rcp, rad (see ACB_PD_scatter_8-29-12)

$$\theta_{pd} := \frac{r_{pdbc}}{L_{arm}}$$

BRDF, sr^-1; CSIRO, surface 2, S/N 2

$$BRDF_1(\theta) := \frac{2755.12}{\left(1 + 8.50787 \cdot 10^8 \cdot \theta^2\right)^{1.23597}}$$

radius of manifold/cryo baffle, m

$$R_{cryo} := \frac{0.769}{2} = 0.385$$

height of ledge, m

$$H_L := 0.769 - 0.655 = 0.114$$

$$H_1 := R_{cryo} - H_L = 0.271$$

radius of ACB hole, m

$$r_{acbhole} := 0.172$$

area of ACB hole, m^2

$$A_h := \pi \cdot r_{acbhole}^{\ 2} = 0.093$$

$$A_h = 0.093$$

thickness of baffle plate, m

$$t := 0.047 \cdot .0254$$

maximum width of exposed edge, m

$$w_e := \frac{t}{\cos\left(33 \cdot \frac{\pi}{180}\right)}$$

$$w_e = 1.423 \times 10^{-3}$$

exposed area of baffle plate hole edge, m^2

$$A_{bpe} := \int_{-r_{acbhole}}^{0} 2 \cdot \sqrt{r_{acbhole}^{\ 2} - x^2}\ dx - \int_{-r_{acbhole}+w_e}^{0} 2 \cdot \sqrt{r_{acbhole}^{\ 2} - (x - w_e)^2}\ dx$$

$$A_{bpe} = 4.897 \times 10^{-4}$$

area of manifold/cryo baffle ledge, m^2

$$A_L := \int_{H_1}^{R_{cryo}} 2 \cdot \sqrt{R_{cryo}^{\ 2} - H^2}\ dH$$

$$A_L = 0.043$$

area of exposed ACB, m^2

$$A_{ACB} := \pi \cdot R_{cryo}^{2} - 2.A_h - A_L = 0.236$$

The intensity of the light incident on the ACB surface is calculated.

power through the cryopump baffle aperture (hits the arm cavity baffle), W

$$P_{acb} := P_a \cdot \int_0^{\theta_{cp}} 2 \cdot \pi \cdot \theta \cdot BRDF_1(\theta) \, d\theta$$

$$P_{acb} = 14.472$$

Area of cryopump baf aperture, m^2

$$A_{cp} := \pi \cdot R_{cp}^{2} = 0.464$$

incident intensity, W/m^2

$$I_i := \frac{P_{acb}}{A_{cp}} = 31.158$$

2.2 Oxidized Stainless Steel Baffle

2.2.1 Scatter from Photodetectors

Scatter from photodetectors

number of photodetector

$$N_{pd} = 16$$

photoconductor area, m^2

$$A_{pd} = 1.021 \times 10^{-4}$$

COC Scattered power hitting the PD, W

$$P_{cocpd} := P_0 \cdot BRDF_1(\theta_{pd}) \cdot \frac{A_{pd}}{L_{arm}^{2}} = 3.706 \times 10^{-3}$$

power scattered by photodetector, into IFO mode, W

$$P_{cocpds} := \sqrt{N_{pd}} \cdot P_{cocpd} \cdot BRDF_{pd} \cdot \frac{\pi \cdot w_{ifo}^{2}}{L_{arm}^{2}} \cdot BRDF_1(\theta_{pd}) \cdot \Delta\Omega_{ifo}$$

$$P_{cocpds} = 7.304 \times 10^{-22}$$

displacement noise @ 100 Hz, m/rtHz

$$DN_{cocpd}(\theta_t) := TF_{itmhr} \cdot \left(\frac{P_{cocpds}}{P_{psl}} \right)^{0.5} \cdot x_{ACB} \cdot \frac{2}{\sqrt{2}} \cdot k$$

$$DN_{cocpd}(\theta_t) = 2.221 \times 10^{-26}$$

2.2.2 Scatter from Screw Heads

Scatter from screw heads

number of screw heads $N_{sh} = 48$

Screw head area, m^2 $A_{sh} = 5.027 \times 10^{-5}$

COC Scattered power hitting the screw head W

$$P_{cocsh} := P_0 \cdot BRDF_1(\theta_{pd}) \cdot \frac{A_{sh}}{L_{arm}^2} = 1.825 \times 10^{-3}$$

power scattered by screw head into IFO mode, W

$$P_{cocshs}(N_{sh}) := \sqrt{N_{sh}} \cdot P_{cocsh} \cdot BRDF_{sh} \cdot \frac{\pi \cdot w_{ifo}^2}{L_{arm}^2} \cdot BRDF_1(\theta_{pd}) \cdot \Delta\Omega_{ifo}$$

$$P_{cocshs}(N_{sh}) = 3.115 \times 10^{-20}$$

displacement noise @ 100 Hz, m/rtHz

$$DN_{cocsh}(\theta_t, N_{sh}) := TF_{itmhr} \cdot \left(\frac{P_{cocshs}(N_{sh})}{P_{psl}} \right)^{0.5} \cdot x_{ACB} \cdot \frac{2}{\sqrt{2}} \cdot k$$

$$DN_{cocsh}(\theta_t, N_{sh}) = 1.45 \times 10^{-25}$$

2.2.3 BRDF of Oxidized Stainless Steel

The incident angle of the light hitting the louver portion of the ACB is 57 deg, and the incident angle hitting the edge of the central plate and the hole of the baffle is centered at approximately 0 deg.

The BRDF, sr^-1 of oxidized polished stainless steel was measured with a CASI scatterometer at incidence angles of 57 deg and 3 deg as a function of the angle away from the specular direction.

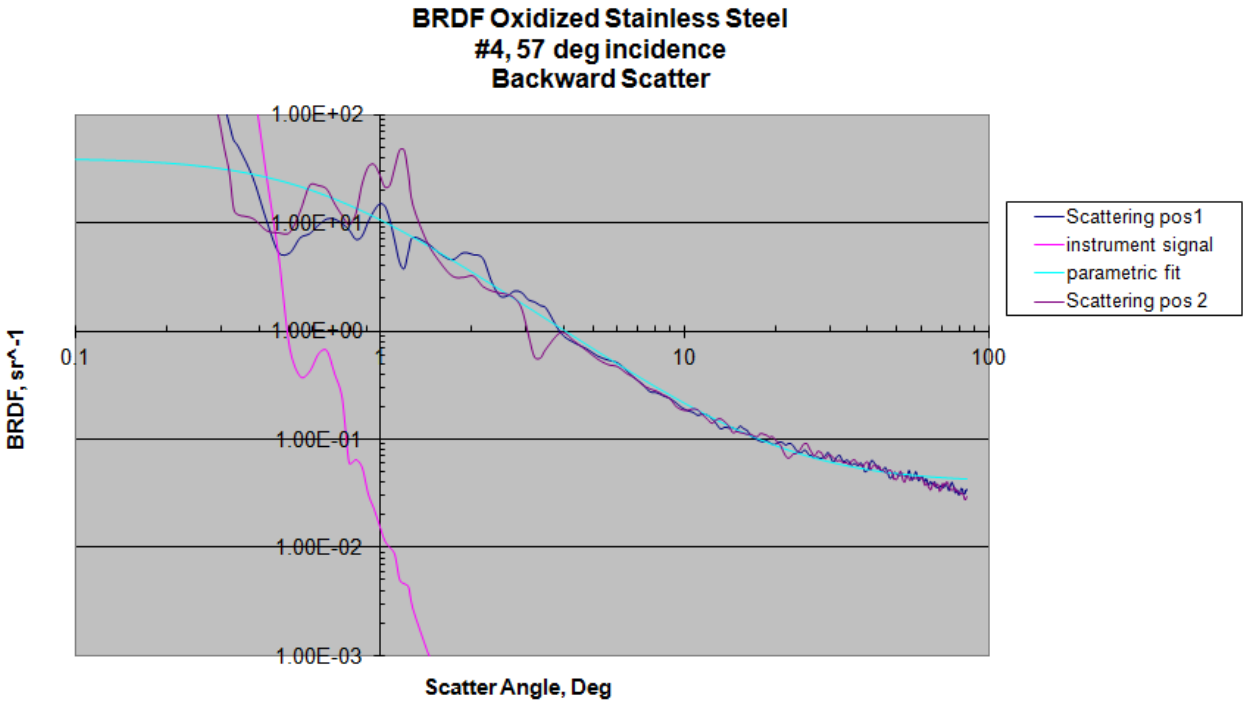

Figure 7: Measured BRDF Data, Oxidized Stainless Steel, with Parametric Fit

The parametric curves shown below were fit to the CASI BRDF data.
The 3 deg data will be used for computing the normal incidence BRDF values. The BRDF data is approximately symmetrical for plus and minus angles about the specular direction.

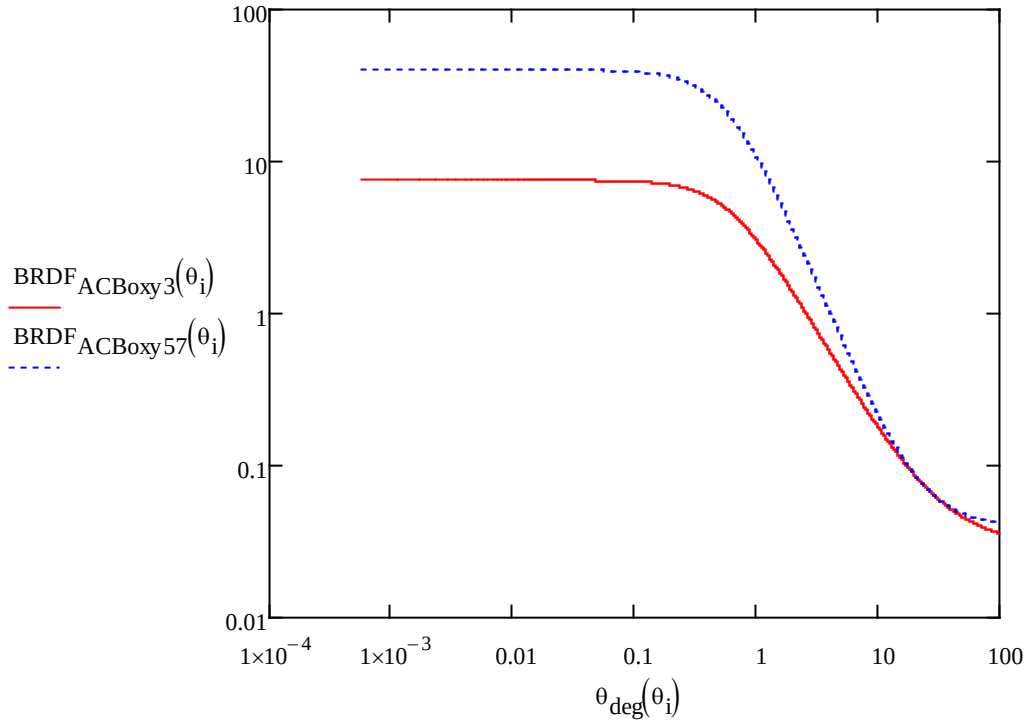

Figure 8: Parametric BRDF Functions, as Best Fit to CASI Data

2.2.4 Scatter by Oxidized SS Baffle Hole Edge

BRDF geometric scatter function from baffle hole edge

$$S_{boxy}(\theta_t, BRDF_{ACBoxy3}) = 7.008 \times 10^{-13}$$

Scattered power into IFO from baffle hole edge

$$P_{acboxyholesifo}(\theta_t) := I_i \cdot A_{bpe} \cdot BRDF_1\left(30 \cdot 10^{-6}\right) \cdot \Delta\Omega_{ifo} \cdot \left(S_{boxy}(\theta_t, BRDF_{ACBoxy3})\right)$$

$$P_{acboxyholesifo}(\theta_t) = 3.651 \times 10^{-20}$$

displacement noise @ 100 Hz, m/rtHz

$$DN_{acboxyhole}(\theta_t) := TF_{itmhr} \cdot \left(\frac{P_{acboxyholesifo}(\theta_t)}{P_{psl}}\right)^{0.5} \cdot x_{ACB} \cdot \frac{2}{\sqrt{2}} \cdot k$$

$$DN_{acboxyhole}(\theta_t) = 1.57 \times 10^{-25}$$

2.2.5 Scatter by Oxidized SS Baffle Center Plate Edge

Scatter from SS center plate edge

power incident on SS center plate edge, W

$$P_{itmbafpedgess} := I_i \cdot A_{ssbp}(r_{edgess})$$

$$P_{itmbafpedgess} = 0.082$$

Scattered power into IFO from oxy SS center plate edge

$$P_{acboxyedgebsifo}(\theta_t, r_{edgess}) := I_i \cdot A_{ssbp}(r_{edgess}) \cdot BRDF_{edgess} \cdot \frac{\pi \cdot w_{ifo}^{2}}{L_{arm}^{2}} \cdot BRDF_1\left(30 \cdot 10^{-6}\right) \cdot \Delta\Omega_{ifo}$$

$$P_{acboxyedgebsifo}(\theta_t, r_{edgess}) = 7.881 \times 10^{-19}$$

displacement noise @ 100 Hz, m/rtHz

$$DN_{acboxyedgeb}(\theta_t, r_{edgess}) := TF_{itmhr} \cdot \left(\frac{P_{acboxyedgebsifo}(\theta_t, r_{edgess})}{P_{psl}}\right)^{0.5} \cdot x_{ACB} \cdot \frac{2}{\sqrt{2}} \cdot k$$

$$DN_{acboxyedgeb}(\theta_t, r_{edgess}) = 7.294 \times 10^{-25}$$

2.2.6 Scatter by Oxidized SS Baffle Bend

BRDF geometric scatter function from oxy baffle bend

$$S_{boxy}(\theta_t, BRDF_{ACBoxy3}) = 7.008 \times 10^{-13}$$

Scattered power into IFO from oxy SS baffle bend

$$P_{acboxybendsifo}(\theta_t, r_{bendss}) := I_i \cdot A_{ssb}(r_{bendss}) \cdot BRDF_1\left(30 \cdot 10^{-6}\right) \cdot \Delta\Omega_{ifo} \cdot \left(S_{boxy}(\theta_t, BRDF_{ACBoxy3})\right)$$

$$P_{acboxybendsifo}(\theta_t, 0.001) = 7.128 \times 10^{-20}$$

displacement noise @ 100 Hz, m/rtHz

$$DN_{acboxybend}(\theta_t, r_{bendss}) := TF_{itmhr} \cdot \left(\frac{P_{acboxybendsifo}(\theta_t, r_{bendss})}{P_{psl}} \right)^{0.5} \cdot x_{ACB} \cdot \frac{2}{\sqrt{2}} \cdot k$$

$$DN_{acboxybend}(\theta_t, 0.001) = 2.194 \times 10^{-25}$$

2.2.7 Scatter by Oxidized SS Louver Baffle Portion

$$BRDF_{ACBoxy57}\left(2 \cdot 57 \cdot \frac{\pi}{180}\right) = 0.042$$

$$P_{acboxylouvsifo} := I_i \cdot A_{ACB} \cdot BRDF_{ACBoxy57}\left(2 \cdot 57 \cdot \frac{\pi}{180}\right) \cdot \frac{\pi \cdot w_{ifo}^{2}}{L_{arm}^{2}} \cdot BRDF_1\left(30 \cdot 10^{-6}\right) \cdot \Delta\Omega_{ifo}$$

$$P_{acboxylouvsifo} = 2.959 \times 10^{-17}$$

displacement noise @ 100 Hz, m/rtHz

$$DN_{acboxylouv}(\theta_t) := TF_{itmhr} \cdot \left(\frac{P_{acboxylouvsifo}}{P_{psl}} \right)^{0.5} \cdot x_{ACB} \cdot \frac{2}{\sqrt{2}} \cdot k$$

$$DN_{acboxylouv}(\theta_t) = 4.47 \times 10^{-24}$$

2.2.8 Total Scatter by Oxidized SS ACB

$$P_{acboxytsifo}(\theta_t, r_{edgess}, r_{bendss}, N_{sh}) = 3.062 \times 10^{-17}$$

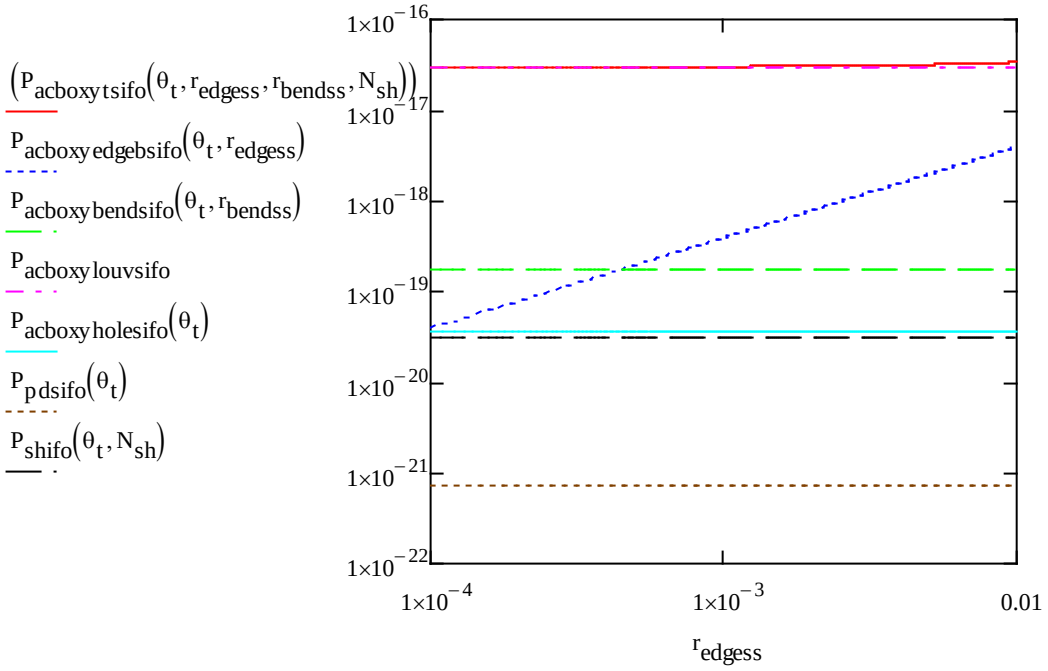

Figure 9: Total Scattered Power, W, by Oxidized SS ACB vs Plate Edge Radius, m

Note: the SS edge scatter does not dominate for edge radius < 0.003 m

total displacement noise @ 100 Hz, m/rtHz

$$DN_{acboxyt}(\theta_t, r_{edgess}, r_{bendss}, N_{sh}) := TF_{itmhr} \cdot \left(\frac{P_{acboxytsifo}(\theta_t, r_{edgess}, r_{edgess}, N_{sh})}{P_{psl}} \right)^{0.5} \cdot x_{ACB} \cdot \frac{2}{\sqrt{2}} \cdot k$$

$$DN_{acboxyt}(\theta_t, r_{edgess}, r_{bendss}, N_{sh}) = 4.477 \times 10^{-24}$$

2.3 Multilayer AR Coating on Stainless Steel

2.3.1 BRDF and Reflectivity of Multilayer AR Coating

The incident angle of the light hitting the louver portion of the ACB is 57 deg, and the incident angle hitting the edge of the central plate and the hole of the baffle is centered at approximately 0 deg.

The BRDF was measured for multilayer AR coating on SS at incidence angles of 57 deg, 30 deg, 15 deg, 10 deg, and 3 deg, as a function of the angle away from the specular direction. The 57 deg data with the parametric fit is shown below.

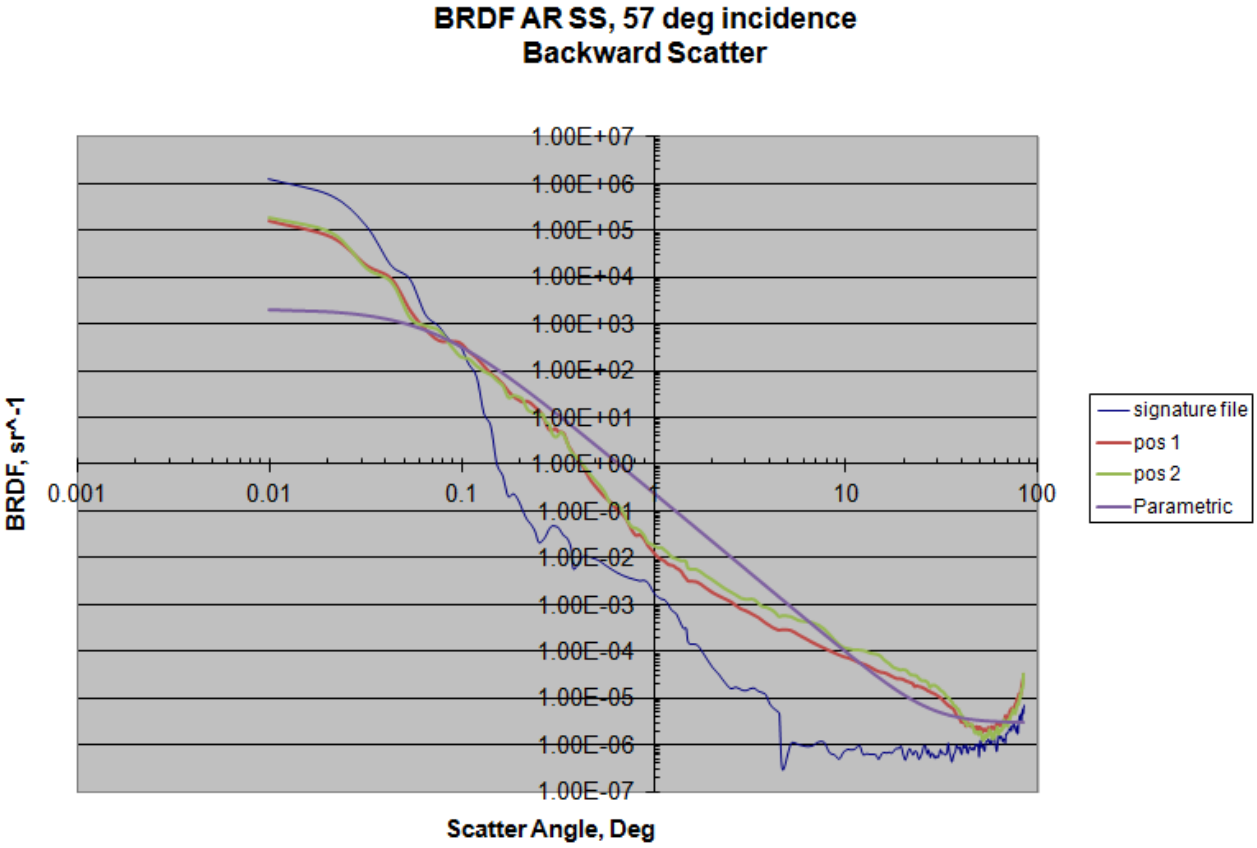

Figure 10: Measured BRDF Data, Multilayer AR Coating on SS, with Parametric Fit

The parametric curves shown below were fit to the CASI BRDF data.

The 3 deg data will be used for computing the normal incidence BRDF values. The BRDF data is approximately symmetrical for plus and minus angles about the specular direction.

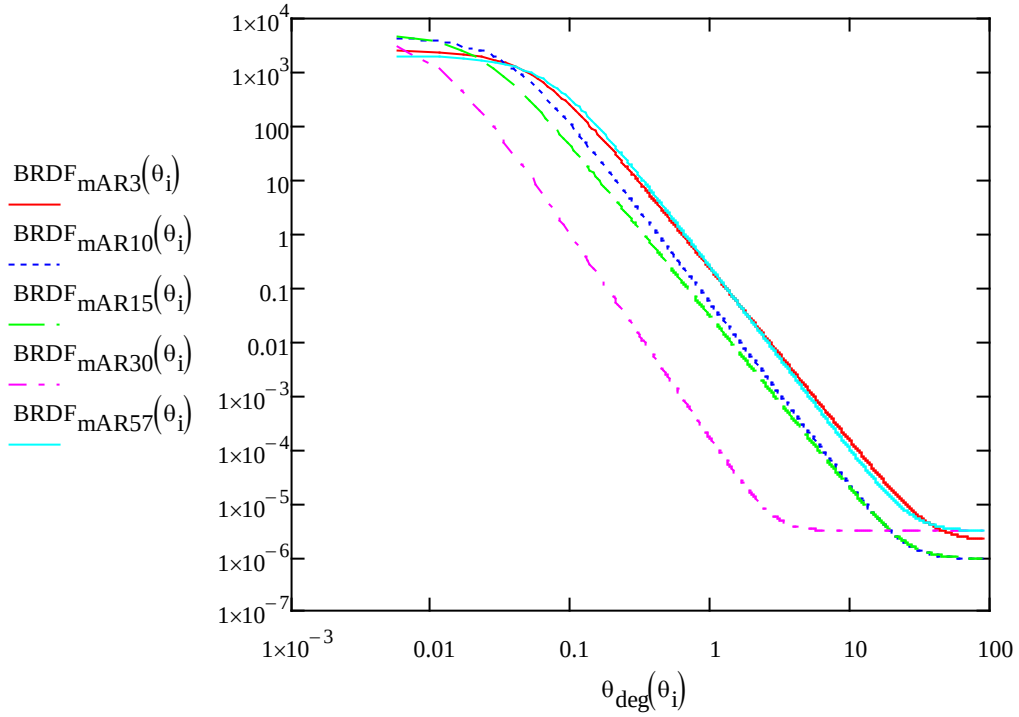

Figure 11: Parametric Functions for Multilayer AR Coating BRDF as Best Fit to CASI Data

Back-scatter BRDF, sr^-1, as a function of incidence angle, deg, is presented below.

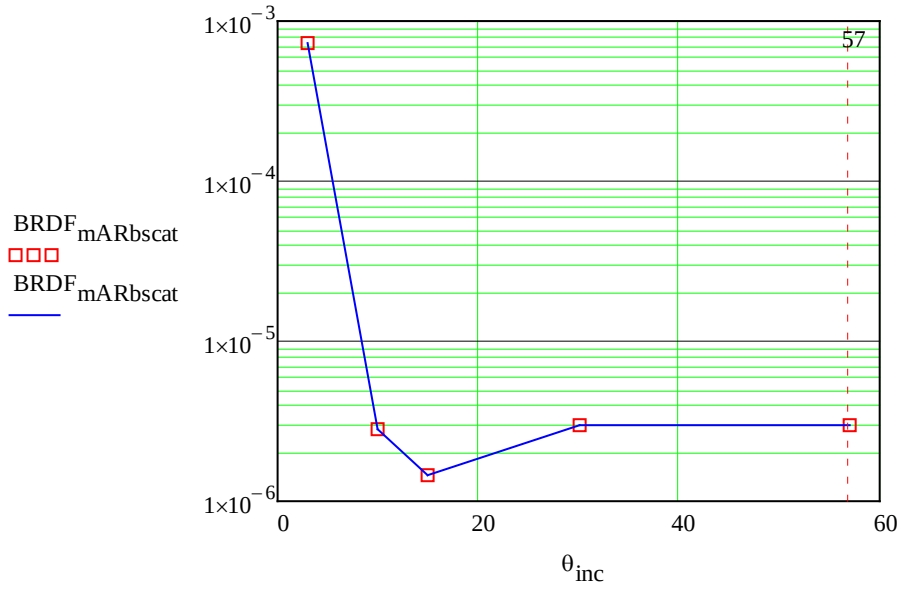

Figure 12: Multilayer AR Coating Backscatter BRDF sr^-1 vs Incidence Angle, Deg

Summary of reflectivity as a function of incidence angle is presented below.

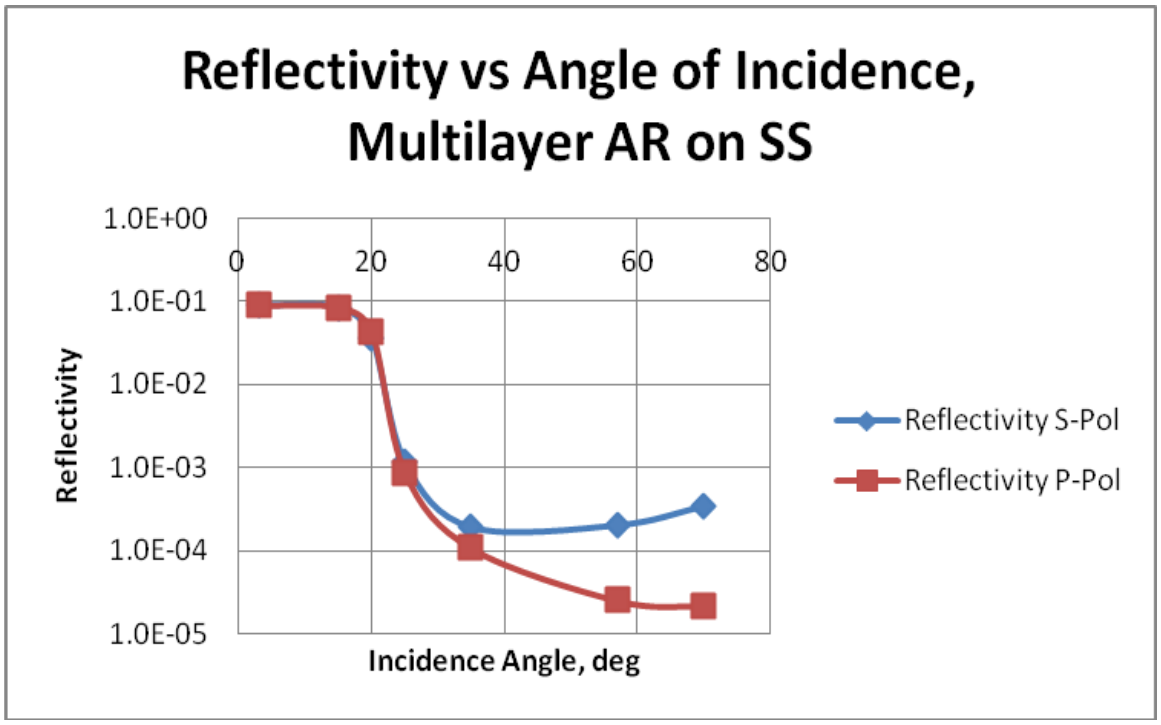

Figure 13: Reflectivity of Multilayer AR Coating vs Incidence Angle

2.3.2 Scatter by Multilayer AR Coating on SS Baffle Hole Edge

Scatter from oxy SS baffle hole edge

BRDF geometric scatter function from baffle hole edge

$$S_{bmAR}(\theta_t, BRDF_{mAR3}) = 7.858 \times 10^{-17}$$

Scattered power into IFO from baffle hole edge

$$P_{acbmARholesifo}(\theta_t) := I_i \cdot A_{bpe} \cdot BRDF_1\left(30 \cdot 10^{-6}\right) \cdot \Delta\Omega_{ifo} \cdot \left(S_{bmAR}(\theta_t, BRDF_{mAR3})\right)$$

$$P_{acbmARholesifo}(\theta_t) = 4.093 \times 10^{-24}$$

displacement noise @ 100 Hz, m/rtHz

$$DN_{acbmARhole}(\theta_t) := TF_{itmhr} \cdot \left(\frac{P_{acbmARholesifo}(\theta_t)}{P_{psl}} \right)^{0.5} \cdot x_{ACB} \cdot \frac{2}{\sqrt{2}} \cdot k$$

$$DN_{acbmARhole}(\theta_t) = 1.662 \times 10^{-27}$$

2.3.3 Scatter by Multilayer AR Coating on SS Center Plate Edge

Scatter from mAR-SS center plate edge

BRDF geometric scatter function from mAR-SS center plate edge

$$S_{emAR}(\theta_t, BRDF_{mAR3}) = 7.858 \times 10^{-17}$$

Scattered power into IFO from mAR-SS baffle center plate edge

$$r_{edgess} = 2 \times 10^{-3}$$

$$P_{acbmARedgebsifo}(\theta_t, r_{edgess}) := I_i \cdot A_{ssbp}(r_{edgess}) \cdot BRDF_1\left(30 \cdot 10^{-6}\right) \cdot \Delta\Omega_{ifo} \cdot \left(S_{emAR}(\theta_t, BRDF_{mAR3})\right)$$

$$P_{acbmARedgebsifo}(\theta_t, r_{edgess}) = 2.19 \times 10^{-23}$$

displacement noise @ 100 Hz, m/rtHz

$$DN_{acbmARedge}\left[\theta_t, (r_{edgess})\right] := TF_{itmhr} \cdot \left[\frac{P_{acbmARedgebsifo}\left[\theta_t, (r_{edgess})\right]}{P_{psl}} \right]^{0.5} \cdot x_{ACB} \cdot \frac{2}{\sqrt{2}} \cdot k$$

$$DN_{acbmARedge}\left[\theta_t, (r_{edgess})\right] = 3.845 \times 10^{-27}$$

2.3.4 Scatter by Multilayer AR Coating on SS Louver Bend

BRDF geometric scatter function from mAR-SS baffle bend

$$S_{bmAR}(\theta_t, BRDF_{mAR3}) = 7.858 \times 10^{-17}$$

Scattered power into IFO from mAR-SS baffle bend

$$P_{acbmARbendsifo}(\theta_t, r_{bendss}) := I_i \cdot A_{ssb}(r_{bendss}) \cdot BRDF_1(30 \cdot 10^{-6}) \cdot \Delta\Omega_{ifo} \cdot (S_{bmAR}(\theta_t, BRDF_{mAR3}))$$

$$P_{acbmARbendsifo}(\theta_t, r_{bendss}) = 1.918 \times 10^{-23}$$

displacement noise @ 100 Hz, m/rtHz

$$DN_{acbmARbend}(\theta_t, r_{bendss}) := TF_{itmhr} \cdot \left(\frac{P_{acbmARbendsifo}(\theta_t, r_{bendss})}{P_{psl}} \right)^{0.5} \cdot x_{ACB} \cdot \frac{2}{\sqrt{2}} \cdot k$$

$$DN_{acbmARbend}(\theta_t, 0.001) = 2.323 \times 10^{-27}$$

2.3.5 Scatter by Multilayer AR Coating on SS Louver Baffle Portion

Power Scattered from the mAR-SS louver portion of baffle

$$BRDF_{mAR57}\left(2 \cdot 57 \cdot \frac{\pi}{180}\right) = 3.025 \times 10^{-6}$$

$$P_{acbmARlouvsifo}(\theta_t) := I_i \cdot A_{ACB} \cdot BRDF_{mAR57}\left(2 \cdot 57 \cdot \frac{\pi}{180}\right) \cdot \frac{\pi \cdot w_{ifo}^2}{L_{arm}^2} \cdot BRDF_1(30 \cdot 10^{-6}) \cdot \Delta\Omega_{ifo}$$

$$P_{acbmARlouvsifo}(\theta_t) = 2.144 \times 10^{-21}$$

displacement noise @ 100 Hz, m/rtHz

$$DN_{acbmARlouv}(\theta_t) := TF_{itmhr} \cdot \left(\frac{P_{acbmARlouvsifo}(\theta_t)}{P_{psl}} \right)^{0.5} \cdot x_{ACB} \cdot \frac{2}{\sqrt{2}} \cdot k$$

$$DN_{acbmARlouv}(\theta_t) = 3.804 \times 10^{-26}$$

2.3.6 Scatter from Screw Heads

See section 2.2.1

2.3.7 Scatter from Photodetectors

See section 2.2.2

2.3.8 Total Scatter by Multilayer AR Coating on SS ACB

Reduce screw head BRDF by polishing so that louver dominates the scatter

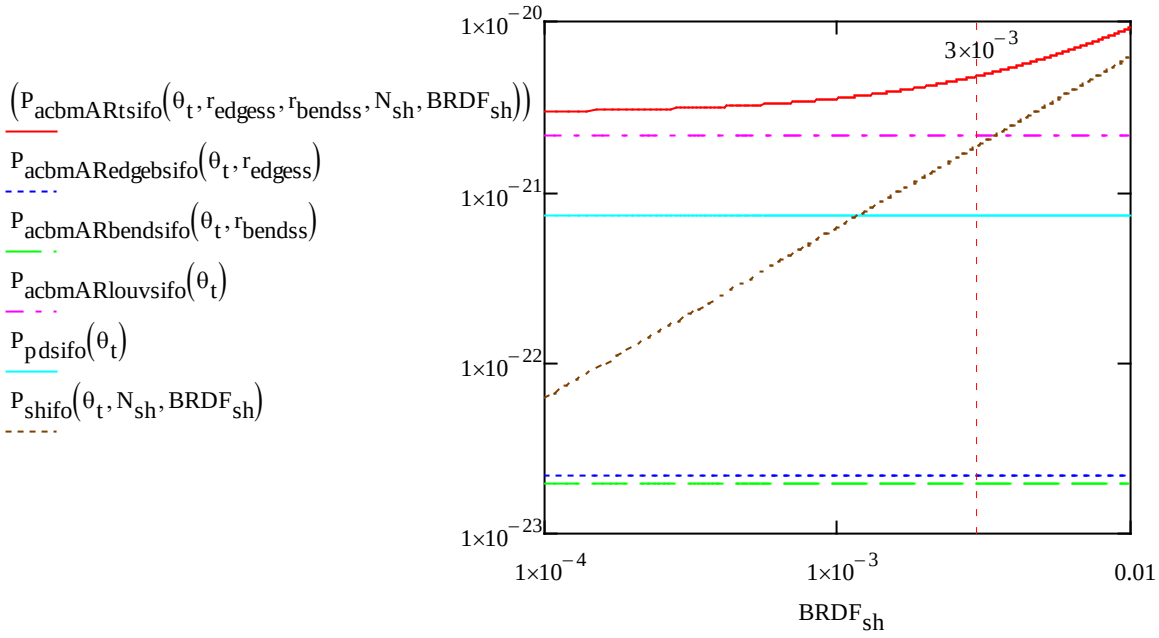

Figure 14: Total Scattered Power, W, by Multilayer AR Coating on SS ACB vs Screw Head BRDF, sr^-1

Note: the screw head BRDF must be < 0.003 sr^-1 for louver scatter to dominate

Tilt the baffle so that edge scatter does not dominate

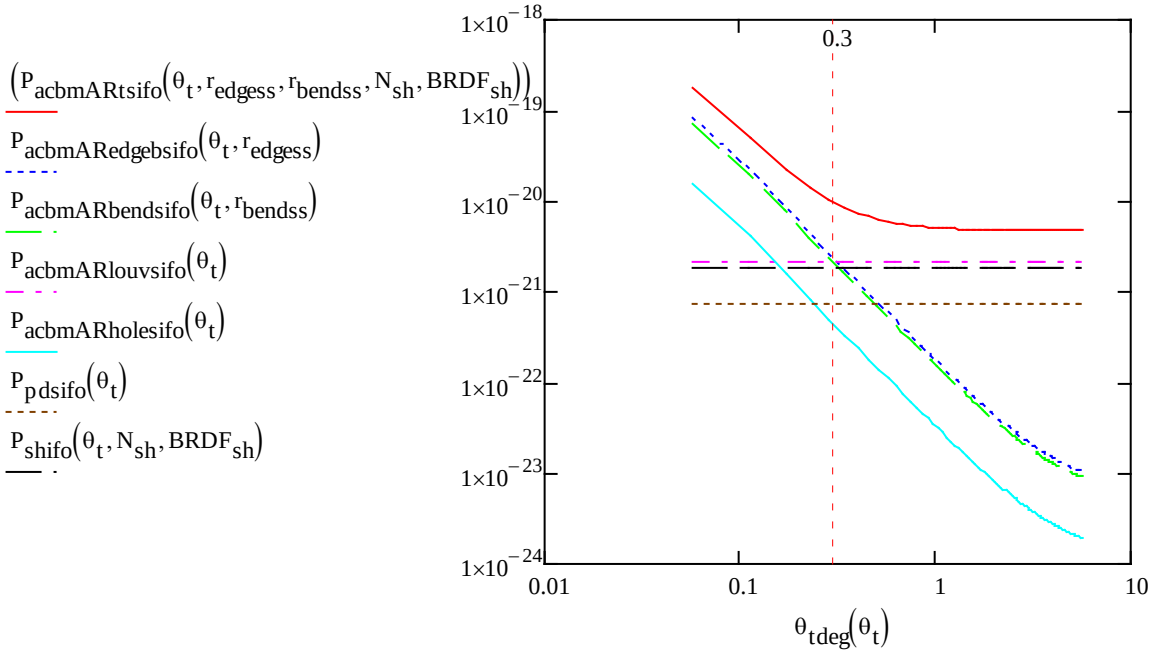

Figure 15: Total Scattered Power, W, by Multilayer AR Coating on SS ACB vs Tilt Angle, Deg

Note: the edge scatter does not dominate for tilt angles >0.3 deg

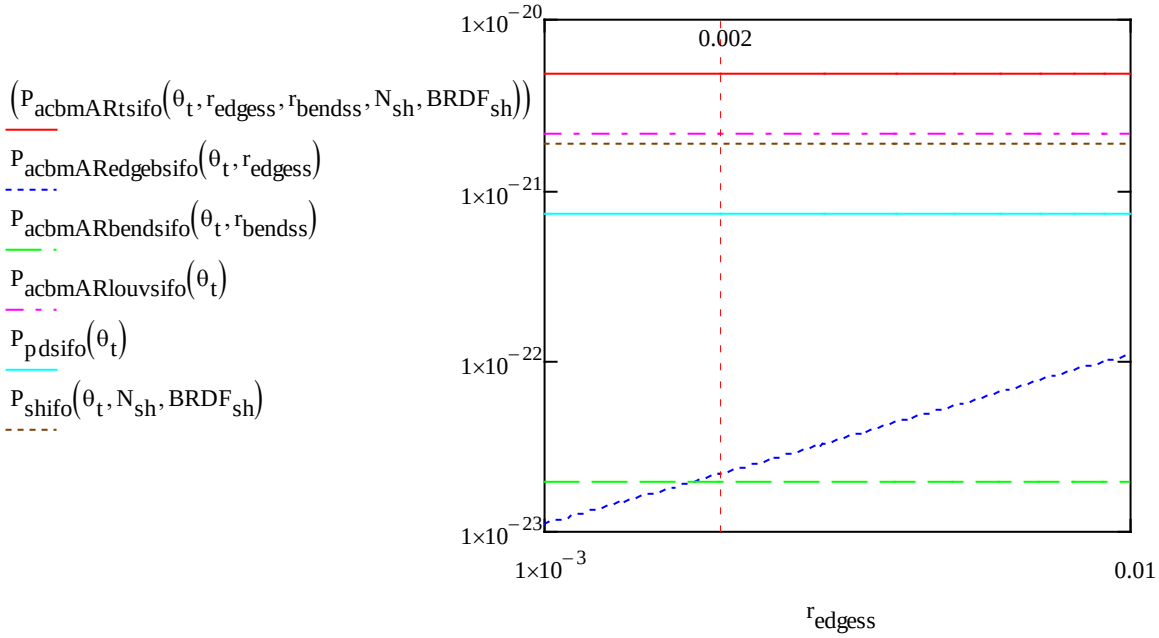

Figure 16: Total Scattered Power, W, by Multilayer AR Coating on SS ACB vs Center Plate Edge Radius, m

Note: the DLC edge scatter does not dominate for edge radius < 0.01 m

total displacement noise @ 100 Hz, m/rtHz

$\theta_t = 0.052$

$r_{edgess} = 2 \times 10^{-3}$

$BRDF_{sh} = 3 \times 10^{-3}$

$$DN_{acbmARt}(\theta_t, r_{edgess}, r_{bendss}, N_{sh}, BRDF_{sh}) := TF_{itmhr} \cdot \left(\frac{P_{acbmARtsifo}(\theta_t, r_{edgess}, r_{bendss}, N_{sh}, BRDF_{sh})}{P_{psl}} \right)^{0.5} \cdot x_{ACB} \cdot \frac{2}{\sqrt{2}} \cdot k$$

$$DN_{acbmARt}(\theta_t, r_{edgess}, r_{bendss}, N_{sh}, BRDF_{sh}) = 5.686 \times 10^{-26}$$

2.4 DLC Coating on Stainless Steel

2.4.1 BRDF and Reflectivity of DLC Coating

The incident angle of the light hitting the louver portion of the ACB is 57 deg, and the incident angle hitting the edge of the central plate and the hole of the baffle is centered at approximately 0 deg.

A DLC AR coating on SS was obtained from R. Takahashi of the KAGRA group. The

properties of this coating were previously reported by R. Takahashi et al. The film was deposited using direct current plasma chemical vapor deposition (CVD), 120 mA @ 500V.

The BRDF was measured for DLC coating on SS at incidence angles of 57 deg and 3 deg as a function of the angle away from the specular directions.

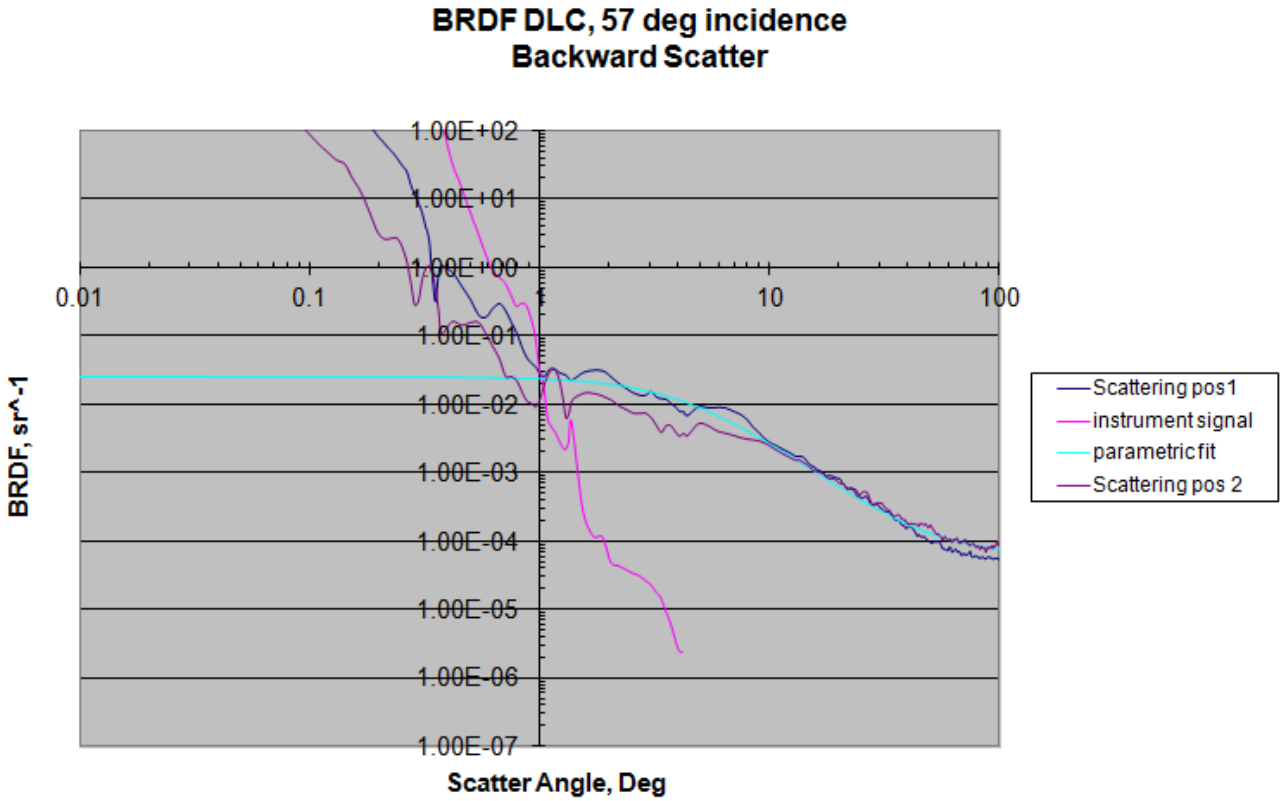

Figure 17: Measured BRDF Data, DLC Coating on SS, with Parametric Fit

The parametric curves shown below were fit to the CASI BRDF data.

The 5 deg data will be used for computing the normal incidence BRDF values. The BRDF data is approximately symmetrical for plus and minus angles about the specular direction.

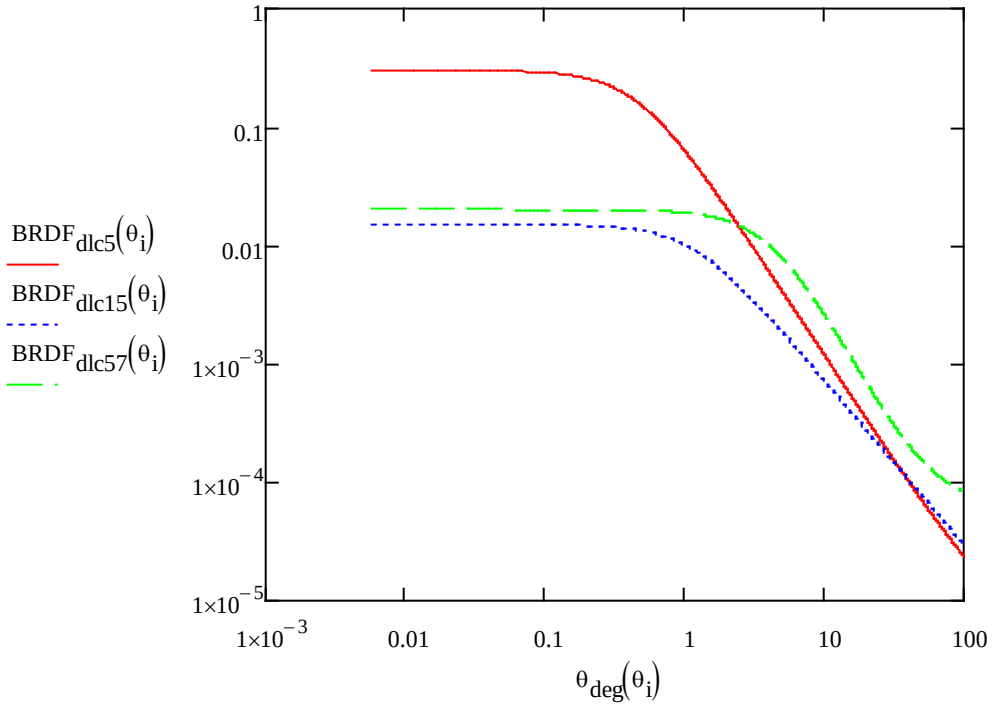

Figure 18: Parametric DLC Coating BRDF Functions, as Best Fit to CASI Data

Back-scatter BRDF, sr^-1, as a function of incidence angle is presented below.

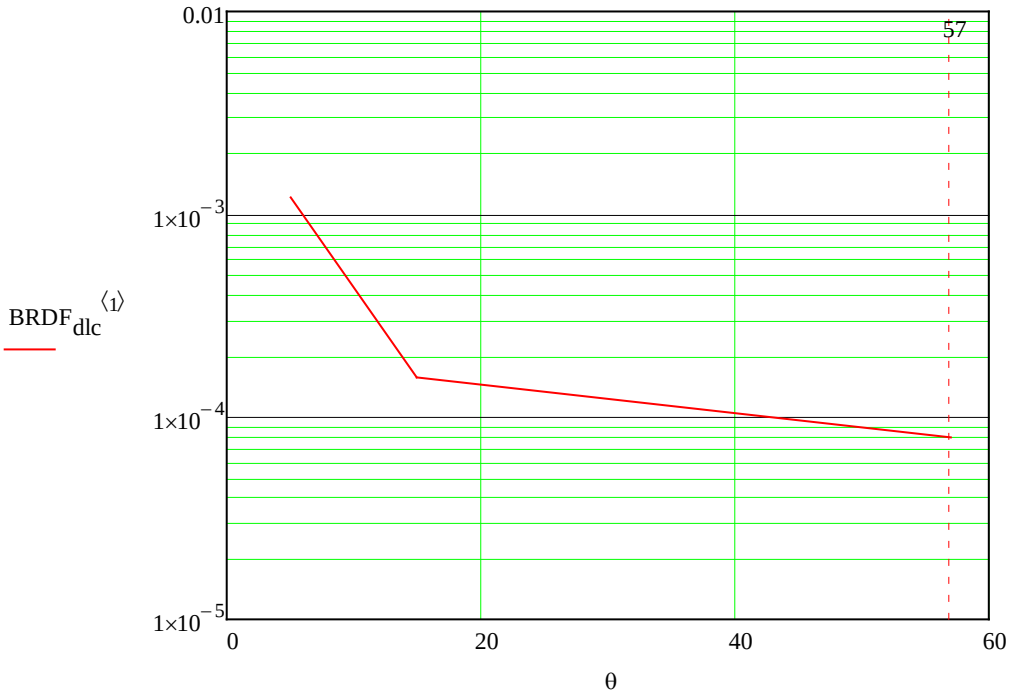

Figure 19: Backscatter BRDF, sr^-1, DLC Coating as a Function of Incidence Angle, Deg

Summary of reflectivity as a function of incidence angle is presented below.

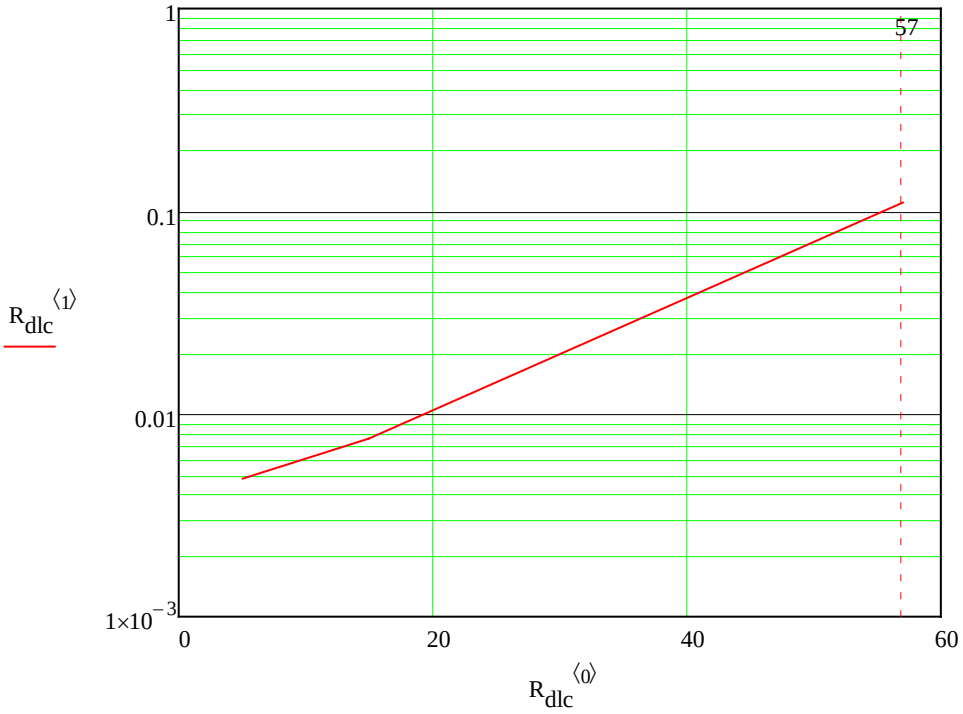

Figure 20: Reflectivity DLC Coating as a Function of Incidence Angle, Deg

2.4.2 Scatter by DLC Coating on SS Baffle Hole Edge

Scatter from DLC SS baffle hole edge

BRDF geometric scatter function from baffle hole edge

$$S_{bdlc}(\theta_t, BRDF_{dlc5}) = 2.766 \times 10^{-15}$$

Scattered power into IFO from baffle hole edge

$$P_{acbdlcholesifo}(\theta_t) := I_i \cdot A_{bpe} \cdot BRDF_1(30 \cdot 10^{-6}) \cdot \Delta\Omega_{ifo} \cdot (S_{bdlc}(\theta_t, BRDF_{dlc5}))$$

$$P_{acbdlcholesifo}(\theta_t) = 1.441 \times 10^{-22}$$

displacement noise @ 100 Hz, m/rtHz

$$DN_{acbdlchole}(\theta_t) := TF_{itmhr} \cdot \left(\frac{P_{acbdlcholesifo}(\theta_t)}{P_{psl}} \right)^{0.5} \cdot x_{ACB} \cdot \frac{2}{\sqrt{2}} \cdot k$$

$$DN_{acbdlchole}(\theta_t) = 9.864 \times 10^{-27}$$

2.4.3 Scatter by DLC Coating on SS Center Plate Edge

Scatter from DLC-SS center plate edge

BRDF geometric scatter function from DLC-SS center plate edge

$$S_{edlc}(\theta_t, BRDF_{dlc5}) = 2.766 \times 10^{-15}$$

Scattered power into IFO from DLC-SS baffle center plate edge

$$r_{edgess} = 2 \times 10^{-3}$$

$$P_{acbdlcedgebsifo}(\theta_t, r_{edgess}) := I_i \cdot A_{ssbp}(r_{edgess}) \cdot BRDF_1(30 \cdot 10^{-6}) \cdot \Delta\Omega_{ifo} \cdot (S_{edlc}(\theta_t, BRDF_{dlc5}))$$

$$P_{acbdlcedgebsifo}(\theta_t, r_{edgess}) = 7.711 \times 10^{-22}$$

displacement noise @ 100 Hz, m/rtHz

$$DN_{acbdlcedge}[\theta_t, (r_{edgess})] := TF_{itmhr} \cdot \left[\frac{P_{acbdlcedgebsifo}[\theta_t, (r_{edgess})]}{P_{psl}} \right]^{0.5} \cdot x_{ACB} \cdot \frac{2}{\sqrt{2}} \cdot k$$

$$DN_{acbdlcedge}[\theta_t, (r_{edgess})] = 2.282 \times 10^{-26}$$

2.4.4 Scatter by DLC Coating on SS Baffle Bend

Scatter from DLC-SS baffle bend

BRDF geometric scatter function from DLC-SS baffle bend

$$S_{bdlc}(\theta_t, BRDF_{dlc5}) = 2.766 \times 10^{-15}$$

Scattered power into IFO from DLC-SS baffle bend

$$P_{acbdlcbendsifo}(\theta_t, r_{bendss}) := I_i \cdot A_{ssb}(r_{bendss}) \cdot BRDF_1\left(30 \cdot 10^{-6}\right) \cdot \Delta\Omega_{ifo} \cdot \left(S_{bdlc}(\theta_t, BRDF_{dlc5})\right)$$

$$P_{acbdlcbendsifo}(\theta_t, 0.001) = 2.814 \times 10^{-22}$$

displacement noise @ 100 Hz, m/rtHz

$$DN_{acbdlcbend}(\theta_t, r_{bendss}) := TF_{itmhr} \cdot \left(\frac{P_{acbdlcbendsifo}(\theta_t, r_{bendss})}{P_{psl}}\right)^{0.5} \cdot x_{ACB} \cdot \frac{2}{\sqrt{2}} \cdot k$$

$$DN_{acbdlcbend}(\theta_t, 0.001) = 1.378 \times 10^{-26}$$

2.4.5 Scatter by DLC Coating on SS Louver Baffle Portion

Power Scattered from the DLC-SS louver portion of baffle

$$BRDF_{dlc57}\left(2.57 \cdot \frac{\pi}{180}\right) = 7.952 \times 10^{-5}$$

$$P_{acbdlclouvsifo}(\theta_t) := I_i \cdot A_{ACB} \cdot BRDF_{dlc57}\left(2.57 \cdot \frac{\pi}{180}\right) \cdot \frac{\pi \cdot w_{ifo}^{2}}{L_{arm}^{2}} \cdot BRDF_1\left(30 \cdot 10^{-6}\right) \cdot \Delta\Omega_{ifo}$$

$$P_{acbdlclouvsifo}(\theta_t) = 5.676 \times 10^{-20}$$

displacement noise @ 100 Hz, m/rtHz

$$DN_{acbdlclouv}(\theta_t) := TF_{itmhr} \cdot \left(\frac{P_{acbdlclouvsifo}(\theta_t)}{P_{psl}} \right)^{0.5} \cdot x_{ACB} \cdot \frac{2}{\sqrt{2}} \cdot k$$

$$DN_{acbdlclouv}(\theta_t) = 1.957 \times 10^{-25}$$

2.4.6 Scatter from Screw Heads

See section 2.2.2

2.4.7 Scatter from Photodetectors

See section 2.2.1.

2.4.8 Total Scatter by DLC Coating on SS ACB

Tilt the baffle so that edge scatter does not dominate

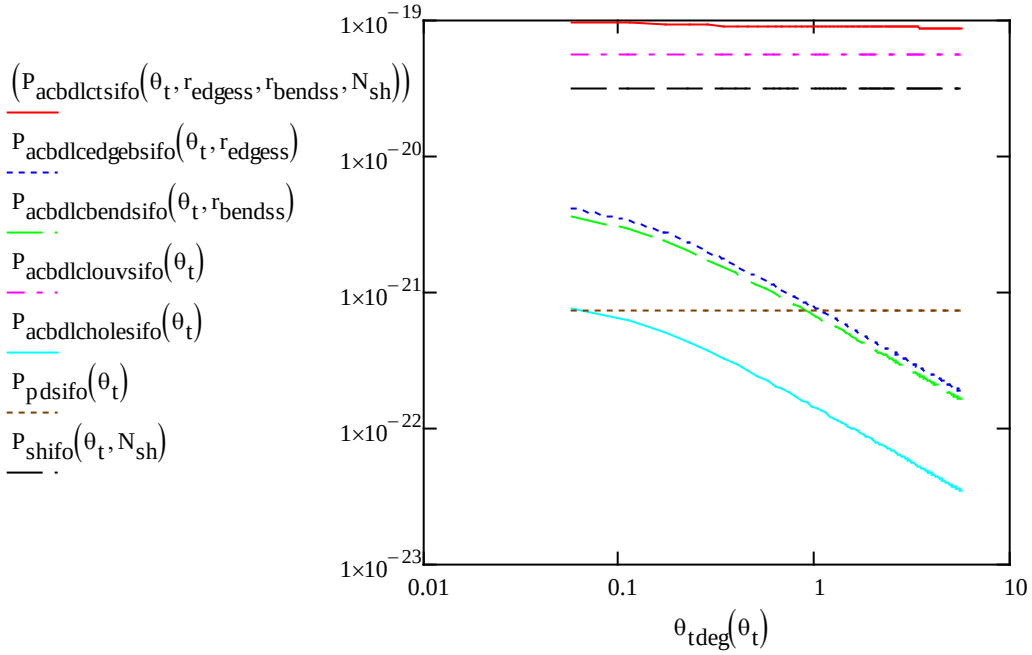

Figure 21: Total Scattered Power, W, by DLC Coating on SS ACB vs Tilt Angle, Deg

Note: the edge scatter does not dominate for tilt angles >1 deg

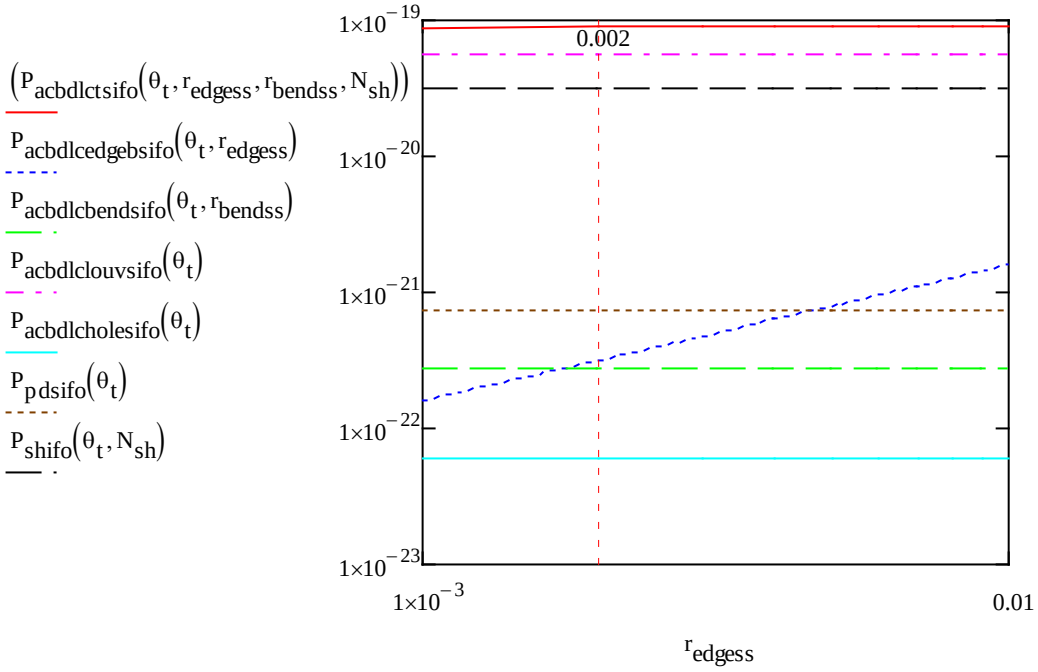

Figure 22: Total Scattered Power, W, by DLC Coating on SS ACB vs Center Plate Edge Radius, m

Note: the DLC edge scatter does not dominate for edge radius < 0.01 m

total displacement noise @ 100 Hz, m/rtHz

$$\theta_t = 0.052$$

$$r_{edgess} = 2 \times 10^{-3}$$

$$DN_{acbdlct}\left(\theta_t, r_{edgess}, r_{bendss}, N_{sh}\right) := TF_{itmhr} \cdot \left(\frac{P_{acbdlctsifo}\left(\theta_t, r_{edgess}, r_{bendss}, N_{sh}\right)}{P_{psl}}\right)^{0.5} \cdot x_{ACB} \cdot \frac{2}{\sqrt{2}} \cdot k$$

$$DN_{acbdlct}\left(\theta_t, r_{edgess}, r_{bendss}, N_{sh}\right) = 2.45 \times 10^{-25}$$

3 Conclusions

3.1 Comparison of Scattered Light Displacement Noise, m/rtHz from Multilayer AR Coating ACB and DLC Coating ACB with Default aLIGO Oxidized SS ACB

Comparison of mAR coated SS to oxidized SS baffle

$$\frac{DN_{acboxyt}(\theta_t, r_{edgess}, r_{bendss}, N_{sh}, BRDF_{sh})}{DN_{acbmARt}(\theta_t, r_{edgess}, r_{bendss}, N_{sh}, BRDF_{sh})} = 79.837$$

Comparison of DLC coated SS to oxidized SS baffle

$$\frac{DN_{acboxyt}(\theta_t, r_{edgess}, r_{bendss}, N_{sh})}{DN_{acbdlct}(\theta_t, r_{edgess}, r_{bendss}, N_{sh})} = 18.539$$

Based on measured BRDF data, a 19 times reduction in scattered light displacement noise could be achieved with the DLC coating, and an 80 times reduction in scattered light displacement noise could be obtained with the multilayer AR coating, in comparison with the default oxidized SS ACB.

3.2 Limiting Scattering Sources

3.2.1 Edge Scatter

The limiting scatter from the frontal edges of the baffle is effectively eliminated by tilting the baffle > 1 deg in the pitch direction.

3.2.2 Screw Head Scatter

Scatter from the three screw heads around the periphery of each photodetector is a limiting scattering source for the case of the multilayer AR coated SS. This limiting scattering source can be eliminated by polishing the surfaces of the flat screw heads to achieve a BRDF <0.003 sr^-1.

3.3 BRDF

The back-scatter BRDF at 57 deg incidence angle of the multilayer AR coating on SS is <1E-5 sr^-1 for p-polarization.

3.4 Reflectivity

The reflectivity at 57 deg incidence angle of the multilayer AR coating on SS is <1E-3 for both polarizations.

4 Reference Data

T1300716-v1_ACB Multi-AR coating on SS
T1300717-v1_BRDF Multi-AR SS 3 deg inc
T1300718-v1_BRDF Multi-AR SS 15 deg inc
T1300719-v1_BRDF Multi-AR SS 57 deg inc
T1300765-v1_BRDF Multi-AR SS 30 deg inc
T1300766-v1_BRDF Multi-AR SS 10 deg inc
T1300768-v1_DLC 5 deg inc
T1300767-v1_DLC 15 deg inc
T1300764-v1_DLC 57 deg inc